Front. Energy 2023, 17(2): 211–227
https://doi.org/10.1007/s11708-022-0847-3

RESEARCH ARTICLE

Hanyi WANG, Renjie LUO, Qun YU, Zhiyi LI

Topology-independent end-to-end learning model for improving the voltage profile in microgrids-integrated power distribution networks

Abstract With multiple microgrids (MGs) integrated into power distribution networks in a distributed manner, the penetration of renewable energy like photovoltaic (PV) power generation surges. However, the operation of power distribution networks is challenged by the issues of multiple power flow directions and voltage security. Accordingly, an efficient voltage control strategy is needed to ensure voltage security against ever-changing operating conditions, especially when the network topology information is absent or inaccurate. In this paper, we propose a novel data-driven voltage profile improvement model, denoted as system-wide composite adaptive network (SCAN), which depends on operational data instead of network topology details in the context of power distribution networks integrated with multiple MGs. Unlike existing studies that realize topology identification and decision-making optimization in sequence, the proposed end-to-end model determines the optimal voltage control decisions in one shot. More specifically, the proposed model consists of four modules, Pre-training Network and modified interior point methods with adversarial networks (Modified IPMAN) as core modules, and discriminator generative adversarial network (Dis-GAN) and Volt convolutional neural network (Volt-CNN) as ancillary modules. In particular, the generator in SCAN is trained by the core modules in sequence so as to form an end-to-end mode from data to decision. Numerical experiments based on IEEE 33-bus and 123-bus systems have validated the effectiveness and efficiency of the proposed method.

Keywords end-to-end learning, microgrids, voltage profile improvement, generative adversarial network

Received Jul. 11, 2022; accepted Oct. 12, 2022; online Dec. 30, 2022

Hanyi WANG, Renjie LUO, Qun YU, Zhiyi LI (✉)
College of Electrical Engineering, Zhejiang University, Hangzhou 310027, China
E-mail: zhiyi@zju.edu.cn

Special Column: Microgrids and Integrated Energy Systems

1 Introduction

To meet environmental concerns, renewable energy resource penetration rates have been soaring in power distribution networks, especially for photovoltaic (PV) power generation. Microgrids (MGs) are ideal for accommodating PV needs and are increasingly prevalent in power distribution networks [1–3], where the power distribution network and MGs serve as the backbone and end nodes, respectively. PV output fluctuations lead to random and varying MG outputs, causing a complicated varying and multi-directional power flow in the power distribution networks, especially at noon with strong sunlight. This volatile power flow poses a challenge to distribution system operators (DSOs), forcing voltages to fluctuate over a wide range on all buses. This voltage profile fluctuation can lead to an increasing probability of too high and too low voltages happening in power distribution networks, damaging the electrical equipment and preventing it from running properly, thereby endangering the operation of power distribution networks. Therefore, DSOs need a control strategy that fits the new operation status.

Generally, engineers use on-load tap changers (OLTCs) and reactive power compensations to tackle these issues [4,5]. This voltage profile improvement (VPI) problem can be solved as a typical optimization problem by changing the problem to a second-order cone programming (SOCP) problem or applying other optimization methods; however, these methods are strongly dependent upon the knowledge of detailed network topology. Unfortunately, power distribution network topologies change variably, and the topology information can be inaccurate at times due to power distribution network expansion. Lacking an accurate topology can result in a lack of constraints reflecting the physical properties of a power distribution network. Improving the voltage profile of power distribution networks without accurate topology information is crucial and usually done in a way

consisting of three separate topics, that is, topology identification [6,7], parameter estimation, and control strategy based on identified topology [8–10]. Notably, the performance of the control strategy will be inescapably influenced by the accuracy of the identified topology. In some scenarios, the voltage quality of several buses is more important than that of other buses; however, since the power system is a highly coupled system, it is not clear how the reliability of these buses can be improved in topology identification. Meanwhile, by having three separate topics instead of one, this research path increases the number of problems to be solved, causing inflexibility.

With the rise of contemporary artificial intelligence (AI), data-driven methods have drawn substantial attention. End-to-end methods are promising and prevailing data-driven methods that intend to solve these problem through one deep learning neural network, aiming at the final objective from the beginning. Therefore, it is possible for these methods to focus specifically on the voltages of certain buses. Additionally, compared with multi-stage methods, the end-to-end procedure reduced the complexity of the problem, leading to a higher flexibility and easier deployment.

Among these studies on end-to-end methods, solving the "predict then optimize (PO)" problems [11–13] has attracted attention from researchers. In these problems, the prediction results affect the constraints or objective function of optimization. The raised problem is a generalized PO problem, which first requires a prediction for the topology. Generally, PO problems are solved via the existing structures within the neural network, especially via the overall loss function. Elmachtoub and Grigas [11] and Mandi et al. [12] focused on PO problems whose objective function coefficients are unknown and required data-based predictions. They proposed and enhanced a novel loss function containing both the deviation of prediction and distance to the optimal solution. Furthermore, Babier et al. [13] targeted PO problems whose constraints cannot be presented in expressions and are thus named hidden constraints and proposed a generative adversarial network (GAN)-based neural network denoted as interior point methods with adversarial networks (IPMAN). The hidden constraints are gradually reconstructed as a discriminator belonging to a Style-GAN, while the generator inside IPMAN is gradually trained to generate optimal or sub-optimal solutions. These previous works focused on a linear problem; however, the VPI problem is nonlinear. Furthermore, due to their Style-GAN structures, the number of scenarios is limited, rendering them unsuitable for the countless number of scenarios in a power system.

PO problems exist throughout power engineering [14–16], and the majority of researchers have focused on the correlation between load forecasting and power dispatch. For example, Han et al. [14] focused on load forecasting by taking the cost of optimal power flow (OPF) into load forecasting and training a deep learning network that can make a more suitable prediction of OPF calculations. Furthermore, Lu et al. [15] studied the load forecasting containing cost and combined it with the economic dispatch problem to propose a model-free end-to-end learning model. Zhang et al. [16] studied the loss function in cost-oriented load forecasting and proposed a piecewise loss function for use in various machine learning models. Although the constraints in these optimization problems are affected by forecasting results, accurate topology is still required. Forecasting results merely influence the factors in constraints whose structures are pellucid; however, in VPI problems without accurate topology, neither the structure nor the number of constraints are clear.

Facing a VPI problem without accurate or detailed topology information, we considered the network topology as hidden constraints and proposed system-wide composite adaptive network (SCAN), based on IPMAN, to overcome limitations in existing studies. SCAN was composed of four modules, including the Pre-training Network, Modified IPMAN, the discriminator generative adversarial network (Dis-GAN), and volt convolutional neural network (Volt-CNN). The first two are core modules and the last two are ancillary modules. This study provides the following technical contributions to the field:

1) An end-to-end data-driven optimization method for the power distribution networks without accurate topology, which can optimize the OLTCs and reactive power compensation output simultaneously under an unlimited number of scenarios.

2) SCAN, which we developed on IPMAN, composed of four modules composited inside, magnifying the physical connections between variables and reinforcing the capability of convergence facing the nonlinear objective function.

3) A two-step training procedure introduced into SCAN, offering additional guidance when there is insufficient training data and overfitting.

The remainder of this paper is organized as follows: Section 2 raises the investigated problems and models them in detail; Section 3 intercalates IPMAN and SCAN; Section 4 comprehensively presents the ancillary SCAN modules; Section 5 demonstrates the core modules of SCAN; Section 6 explores IEEE 33- and 123-bus system case studies; and Section 7 poses our conclusions.

2 VPI modeling for power distribution network integrated with MGs

In this Section, the influence of MGs on power distribution networks are investigated, especially the voltage profile uncertainty. Furthermore, the VPI

problem is precisely modeled as an optimization problem, and its complexity is also proposed in this Section.

2.1 Functionality and influences of MGs

Since MG operators and DSOs are unique entities, we considered that MGs have low controllability and are highly dependent on the environment. An MG usually contains three parts, that is, loads, energy storage systems (ESSs), and distributed generations (DGs) [17]; however, because of their high cost, the ESS capacities are quite small compared to the loads and DGs in practical planning. Consequently, we omitted the ESS in the modeling of MGs. The DGs inside an MG consist of many generators, of which PVs account for a large proportion. Given that a power distribution network normally encompasses a small area, PV power generation inside various MGs shares the same light intensity.

For the operation paradigm, grid-forming and grid-following are two prevalent MG choices [18,19]. Grid-forming is predominantly used in islanded MGs that need to maintain a fixed voltage level, while grid-following is predominantly used in a strong grid [20] where the MGs can be recognized as current sources. The relatively cheap cost and simplicity of grid-following has made it widely used in the integration of MGs in a power distribution network [21,22]. Moreover, without converter-generated inertia, grid-following MGs have fast responses, which are also a pertinent safety point for DSOs. Thus, to mimic the actual application scenario, we assumed that all the MGs operated in the grid-following mode. Accordingly, when PV output was high, MGs are randomly fluctuating power injection sources for the power distribution network, whose injection amounts are approximately dominated by the light intensity. Moreover, the power flow inside the power distribution network may frequently change due to the varying power outputs of PVs inside MGs, as illustrated in Fig. 1.

With MG integration, the power flow direction was not fixed, which brings uncertainty to the voltage profile. The voltages of all buses fluctuate in a relatively large range, meaning that a targeted operation strategy is required.

2.2 VPI-based operational decision-making

In DSOs, there are two primary ways to improve the voltage profile of the power distribution network, namely OLTCs and reactive power compensations such as static var compensators and generators (SVCs and SVGs, respectively). These controller outputs are generally solved as an optimization problem, with the operational decision being the optimal solution; therefore, we first modeled the VPI problem.

2.2.1 Objective function

The objective function is simpler than the form of the norm or absolute value, consisting of a sum-of-squares with a linear derivative, as follows:

$$\min \sum_{m=1}^{n} \beta_m (V_m - V_{m0})^2, \tag{1}$$

where n is the number of buses in a power distribution network, V_m is the voltage at bus m, V_{m0} is the nominal voltage at bus m, and β_m is a weighting factor reflecting the importance of the voltage quality at bus m.

Due to the low voltage level in the power distribution networks, the power loss is more significant than that in transmission networks and largely affects the economy of a power distribution network; however, economy is one of the most concerned indicators in DSO [8,9,23,24]. Thus, we also introduce power loss as one of the objectives, forming a multi-objective function f_{obj} that embodies both security and economic indicators of power distribution networks, as follows:

$$\min f_{\text{obj}} = \sum_{m=1}^{n} \beta_m (V_m - V_{m0})^2 + \alpha P_{\text{loss}}, \tag{2}$$

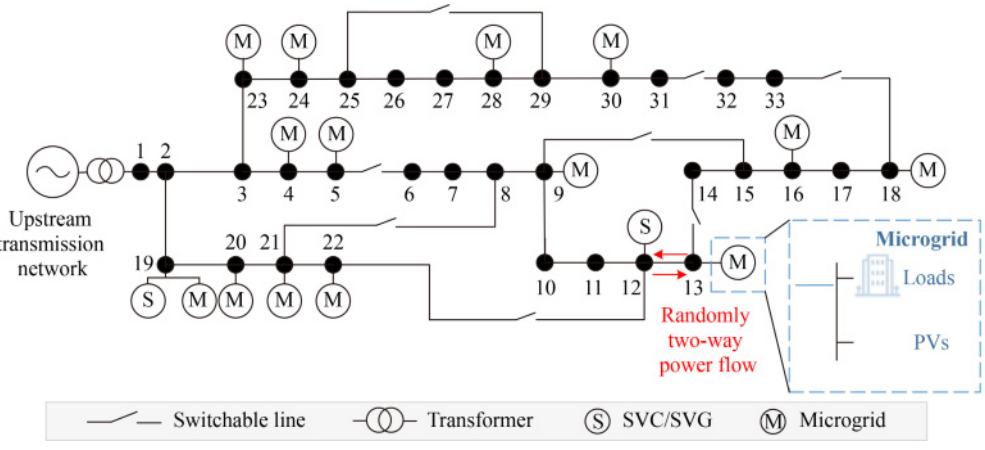

Fig. 1 A power distribution network integrated with MGs.

where P_{loss} is the active power loss in this power distribution network and α is a weighting factor, which allowed the two objectives to be merged together.

2.2.2 Constraints

Unlike typical VPI optimization, not all power distribution network constraints can be written correctly in the equations without accurate topology information. With inaccurate topology, since the bus connection remains unelucidated, it is unrealistic to write constraints that exhibit relevance among buses in equations. For DSOs, a power distribution network without accurate topology is a set of buses whose interconnections are uncertain, that is, it is unfathomable how the buses are coupled or how other buses respond after applying control on one bus. The control strategy is thus up to instincts or experience, which are not reliable or trustworthy, especially under abnormal operating conditions. Consequently, those topology-dependent constraints are hidden constraints in the raised VPI problem.

Hidden constraints contain power flow constraints and constraints of substations with OLTC [25], both of which are fully established on the topology, rendering them impractical for precise mathematical manifestation in the absence of an accurate topology. These hidden constraints are linked to the physical characteristics of power distribution networks in the raised VPI problem, which accounts for most of the constraints.

The explicit constraints are voltage, power loss, SVC/SVG, and power factor constraints, which are further explored here.

a) Voltage constraints

To guarantee the normal operation of electrical equipment, the voltage at each bus should not deviate substantially from the standard value.

$$\underline{V_m} \leqslant V_m \leqslant \overline{V_m}, \tag{3}$$

where $\overline{V_m}$ and $\underline{V_m}$ stand for the upper and lower limits of V_m, respectively.

b) Power loss constraints

Multi-objective optimization can favor one objective too much, so power loss constraints are introduced into this problem, as follows:

$$\begin{aligned} P_{\text{loss}}^{\text{pct}} &\leqslant \overline{P_{\text{loss}}^{\text{pct}}}, \\ Q_{\text{loss}}^{\text{pct}} &\leqslant \overline{Q_{\text{loss}}^{\text{pct}}}, \end{aligned} \tag{4}$$

where $P_{\text{loss}}^{\text{pct}}$ and $Q_{\text{loss}}^{\text{pct}}$ stand for the active and reactive power loss ratios, respectively, which are calculated as Eq. (5); where $\overline{P_{\text{loss}}^{\text{pct}}}$ and $\overline{Q_{\text{loss}}^{\text{pct}}}$ stand for the upper limits of $P_{\text{loss}}^{\text{pct}}$ and $Q_{\text{loss}}^{\text{pct}}$, respectively.

$$\begin{aligned} P_{\text{loss}}^{\text{pct}} &= \frac{P_{\text{inject}} + \alpha_{\text{light}} P_{\text{PV}} - \sum_{l=1}^{n} P_{\text{load},m}}{P_{\text{inject}} + \alpha_{\text{light}} P_{\text{PV}}} \times 100\%, \\ Q_{\text{loss}}^{\text{pct}} &= \frac{Q_{\text{inject}} + \sum_{l=1}^{n} Q_m^{\text{SVC}} + \sum_{l=1}^{n} Q_m^{\text{SVG}} - \sum_{l=1}^{n} Q_{\text{load},m}}{Q_{\text{inject}} + \sum_{l=1}^{n} Q_m^{\text{SVC}} + \sum_{l=1}^{n} Q_m^{\text{SVG}}} \times 100\%, \end{aligned} \tag{5}$$

where P_{inject} represents the active power injected from the upstream transmission network, α_{light} represents the light intensity, P_{PV} represents the sum of capacities of PVs in a power distribution network, $P_{\text{load},m}$ represents the active load at bus m, Q_{inject} represents the reactive power injected from the upstream transmission network, $Q_{\text{load},m}$ represents the reactive load at bus m, and Q_m^{SVC} and Q_m^{SVG} represent the SVC and SVG output at bus m, respectively.

c) SVC/SVG constraints

Each SVC/SVG has its own upper and lower output limits.

$$\begin{aligned} \underline{Q_m^{\text{SVC}}} \leqslant Q_m^{\text{SVC}} \leqslant \overline{Q_m^{\text{SVC}}}, \\ \underline{Q_m^{\text{SVG}}} \leqslant Q_m^{\text{SVG}} \leqslant \overline{Q_m^{\text{SVG}}}, \end{aligned} \tag{6}$$

where $\overline{Q_m^{\text{SVC}}}$ and $\underline{Q_m^{\text{SVC}}}$ are the upper and lower limit of SVC at bus m, respectively; $\overline{Q_m^{\text{SVG}}}$ and $\underline{Q_m^{\text{SVG}}}$ are the upper and lower limit of SVG at bus m, respectively.

d) Power factor constraint

Owing to security and economic issues, the power distribution network, which can be considered a load from the upstream transmission network, is supposed to maintain a high level of power factor.

$$\begin{aligned} \cos\varphi &\geqslant \underline{\cos\varphi}, \\ \cos\varphi &= \frac{P_{\text{inject}}}{\sqrt{P_{\text{inject}}^2 + Q_{\text{inject}}^2}}, \end{aligned} \tag{7}$$

where $\cos\varphi$ is the power factor of the power distribution network, and $\underline{\cos\varphi}$ is the lower limit of $\cos\varphi$.

All in all, this optimization problem can be represented as follows:

$$\min f_{obj} = \sum_{m=1}^{n} \beta_m (V_m - V_{m0})^2 + \alpha P_{\text{loss}},$$

$$s.t. \begin{cases} \text{hidden constraints} \begin{cases} \text{power flow constraints,} \\ \text{substation OLTC constraints,} \end{cases} \\ \text{explicit constraints} \begin{cases} \text{voltage constriants,} \\ \text{active/reactive power loss constraints,} \\ \text{SVC/SVG constraints,} \\ \text{power factor constraint.} \end{cases} \end{cases} \tag{8}$$

2.3 Computational complexity of the proposed model

Generally, for an optimization problem in power

distribution networks, it is common to change it into SOCP [26–28] by applying relaxation to the power flow equations; however, this is only feasible when the optimization model is clear. Since hidden constraints exist in the raised VPI problem (Eq. (8)), DSO can only draw on their engineering experience to maintain the voltage security of the power distribution network, making the control strategy extremely dependent on certain operators.

To give a control strategy that is independent of certain operators, it is possible to draw those hidden constraints based on historical data. In an end-to-end manner, it can instantly draw hidden constraints and search for the optimal decision; however, in actual operation, there are no decisions that violate hidden constraints. It is inapplicable to draw the hidden constraints by comparing feasible and infeasible data, where feasible data means the data satisfying constraints. Furthermore, most explicit constraints are simple upper and lower boundary constraints used to guide normalization. The rest one, that is, the power factor constraint (Eq. (7)), purely focuses on the active and reactive injected power, which is a tiny part of all decision variables. Also, in the absence of an accurate topology, there is no correlation between decision variables, resulting in the fact that most of those variables are not constrained.

3 Structure of IPMAN and SCAN

In this Section, we introduce the structure of the end-to-end method developed for solving optimization problems with hidden constraints, that is, IPMAN. Then considering its deficiencies, we propose and introduce SCAN, that is, a novel composite end-to-end model that can solve the raised VPI problem.

3.1 Basic structure of IPMAN

The main purpose of IPMAN is to generate an approximate optimal solution via GAN, as shown in Fig. 2. IPMAN learns hidden constraints from the existing decision vector x and its corresponding scenario vector u as a training data set, to train a generator $F(u)$, which can generate approximate optimal decisions on scenarios. In the raised VPI problem, x contains OLTCs, SVC/SVG output, controlled voltage profile, and active power loss; and u contains light intensity, active power load, reactive power load, and voltage profile before control.

The oracle $\boldsymbol{\Psi}$ is a discriminatory criterion made up of explicit constraints, to judge whether the generated decision is feasible or not under explicit constraints. The dual parameter λ_j is a variable to balance the feasibility of hidden constraints and optimality. $\{\lambda_j\}_{j=0}^{J}$ is a set of λ_j from λ_0 to λ_J, where J is the number of λ_j in the set. $\{F_j(u)\}_{j=0}^{J}$ is a set of $F^j(u)$ from $F^0(u)$ to $F^J(u)$, where $F^j(u)$ is the generator based on λ_j.

The IPMAN training process is demonstrated in Fig. 3. Under most scenarios, all data are feasible, rendering D as an empty set; therefore, a pre-training GAN was introduced to generate infeasible data set while accelerating the IPMAN training process. For better performance, a Style-GAN [29] was chosen to act as the pre-training GAN, whose loss function is formulated in Eq. (9), where the loss function L_{ST} consists of two parts, that is, the binary cross-entropy of discriminator D_{GAN}, and mean square error (MSE) of generator F. Parameter λ_{ST} is introduced to raise the importance of MSE.

$$\min_{F}\max_{D_{\mathrm{GAN}}}\Bigg\{L_{\mathrm{ST}}:=\frac{1}{N_{\mathrm{u}}}\sum_{(x_i,u_i)\in D}[\log D_{\mathrm{GAN}}(x_i,u_i)+\log(1-D_{\mathrm{GAN}}(F(u_i),u_i))]+\lambda_{\mathrm{ST}}\|F(u_i)-x_i\|_1\Bigg\}, \tag{9}$$

where (x_i, u_i) is the ith piece of data in feasible data set D, N_u is the number of (x_i, u_i) in D.

After Pre-training, the generator F continues to be trained in IPMAN, and the classifier $B^{(k)}$ classifies feasible and infeasible decisions and is re-trained in each

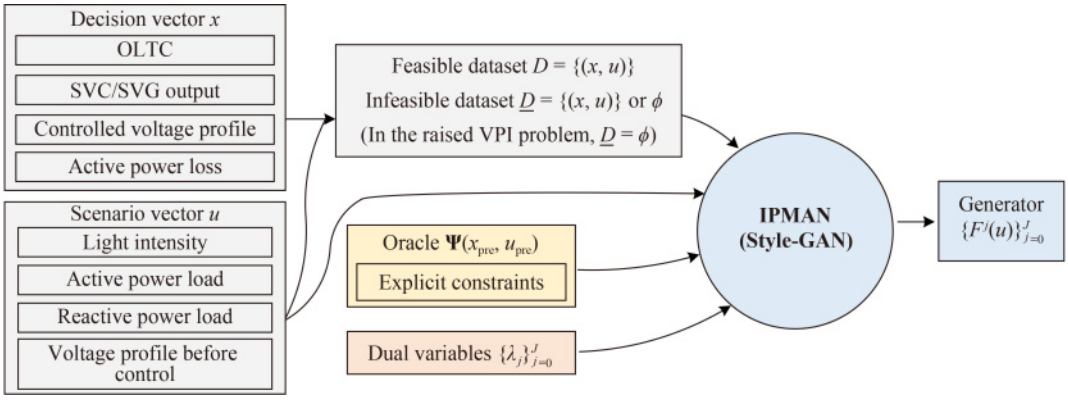

Fig. 2 Input and output of IPMAN.

generation on the newly augmented training data set, to carve the feasibility boundary precisely, as depicted in Fig. 4. Additionally, it assists classifier B in being able to classify the latest data generated by $F^{(k)}$. Here, $F^{(k)}$ refers to the generator F trained in kth generation. Compared with carving the boundary in advance, progressive carving is more comprehensible for $F^{(k)}$ in training and can produce a more precise boundary as it is in a GAN style.

The loss function of F in IPMAN is formulated as Eq. (10), where L_F consists of three parts, that is, the objective function value f_{obj}, the difference between the generated decision and true decision, and the output value of the classifier. To minimize L_F, $F^{(k)}$ needs to reduce the value of f_{obj} while keeping generated decision vector $x_{\text{IPMAN}} = F^{(k)}(u_i)$ feasible.

$$\min_{F\in\mathcal{F}}\left\{L_F := \frac{1}{N_{\text{u}}}\sum_{u_i\in U}\left(\lambda_j f_{\text{obj}}(F(u_i),u_i) + \lambda_{\text{ST}}\|F(u_i)-x_i\|_1 - \sum_{r\in\text{R}}\left[B^{(k)}(F(u_i),u_i)\right]_r\right)\right\}. \tag{10}$$

3.2 Functional framework of SCAN

Among the explicit constraints in the raised VPI problem (Eq. (8)), only the power factor constraint (Eq. (7)) is not embodied in normalization; therefore, it is the only constraint that can be used as the oracle $\boldsymbol{\Psi}$. Additionally,

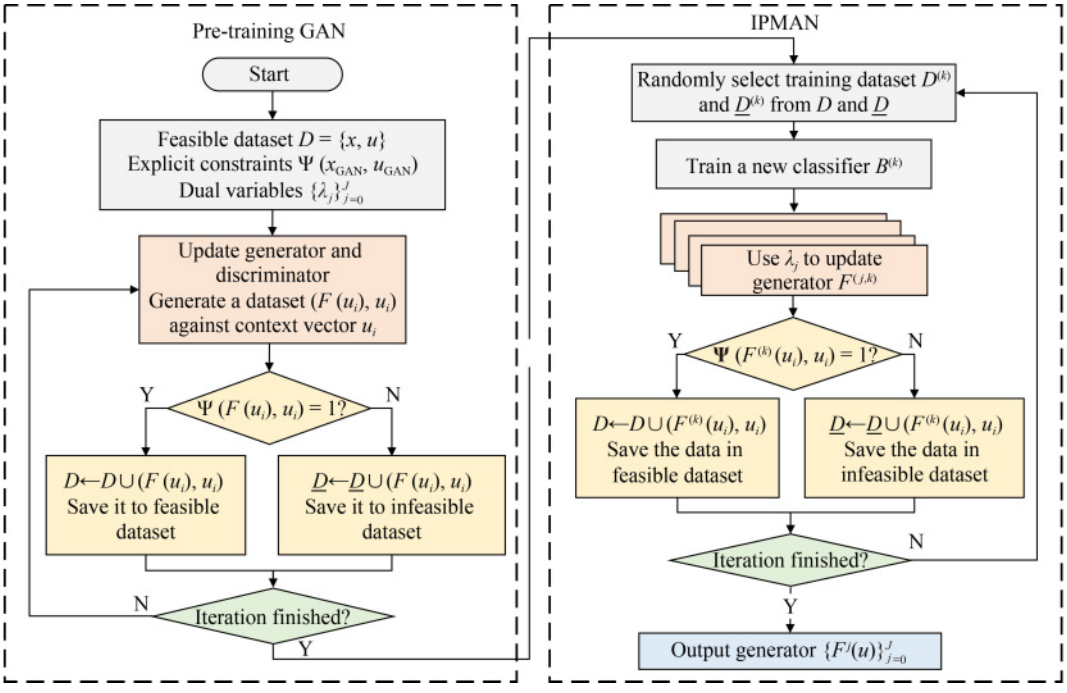

Fig. 3 Training process of IPMAN.

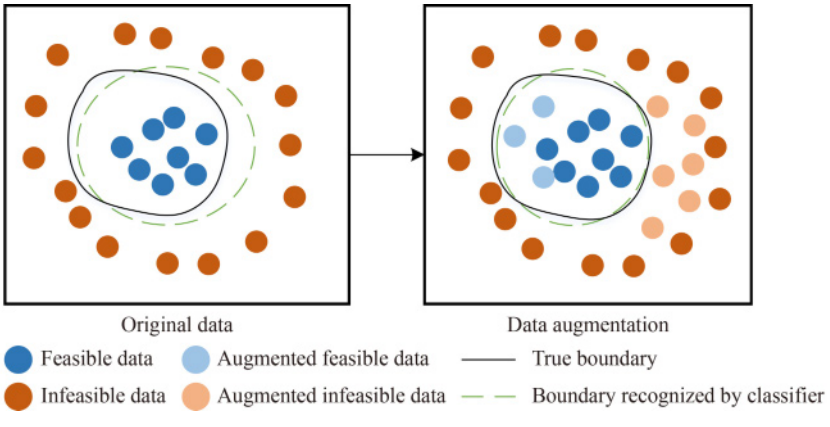

Fig. 4 Progressively carving the feasibility boundary.

this constraint focuses only on the injected active and reactive power and does not constrain most decision variables. Although, theoretically, an oracle $\boldsymbol{\Psi}$ made of even one constraint still makes sense in IPMAN, it is difficult for classifier B to learn a classification that is decided by only a few variables instead of all variables, which leads to a high probability of overfitting. A constraint that focuses on all variables is crucial to oracle $\boldsymbol{\Psi}$.

Furthermore, since each sample generated by F in each generation is checked by true decisions in the second part of L_F, IPMAN takes advantage of the Style-GAN structure, resulting in a better performance; however, this leads to a limited number of scenarios. That is, for each x_i that is generated to a certain existing scenario vector u_i, IPMAN is not able to generate reliable x_i to a new scenario vector. Nevertheless, the scenario vector types are countless for most issues, especially the VPI problem, where both loads and light intensity fluctuate randomly. Additionally, machine learning is a data-driven method that requires a considerable amount of data. Yet in the VPI problem, the decision vector x_i and the scenario vector u_i share a one-to-one correlation. The data are insufficient for Style-GAN to recognize each style.

SCAN (Fig. 5) was proposed to address these defects in the contemporary IPMAN model. The SCAN input and output are the same as IPMAN, meaning that the input data comes from the historical data of empirical decisions. Different from IPMAN, decision vector x is divided into a controller vector y and controlled vector z in SCAN. The deviation of x would significantly enhance the precision and reliability of the SCAN-generated decisions. The workflow of SCAN is stated as follows:

1) The input data were sent to train the ancillary modules, that is, Dis-GAN and Volt-CNN. Dis-GAN is a semi-supervised GAN (Semi-GAN) generating x on u, whose trained discriminator is preoccupied with Eq. (7) as oracle $\boldsymbol{\Psi}$ to overcome the insufficiency of explicit constraints. Volt-CNN is built in a CNN structure, generating z on u and y. As the voltage calculator $\boldsymbol{\Theta}$, Volt-CNN rebuilds the physical correlation between all above variables.

2) Then, as the input data are all feasible data, a Pre-training Network is introduced into SCAN, generating y on u. The voltage calculator $\boldsymbol{\Theta}$ calculates z on u and the generated y. Here, a decision vector x is made up of y and its corresponding z, and each generated x is judged by $\boldsymbol{\Psi}$ to clarify whether it is feasible or not to u. Here, infeasible data are generated by Pre-training Network.

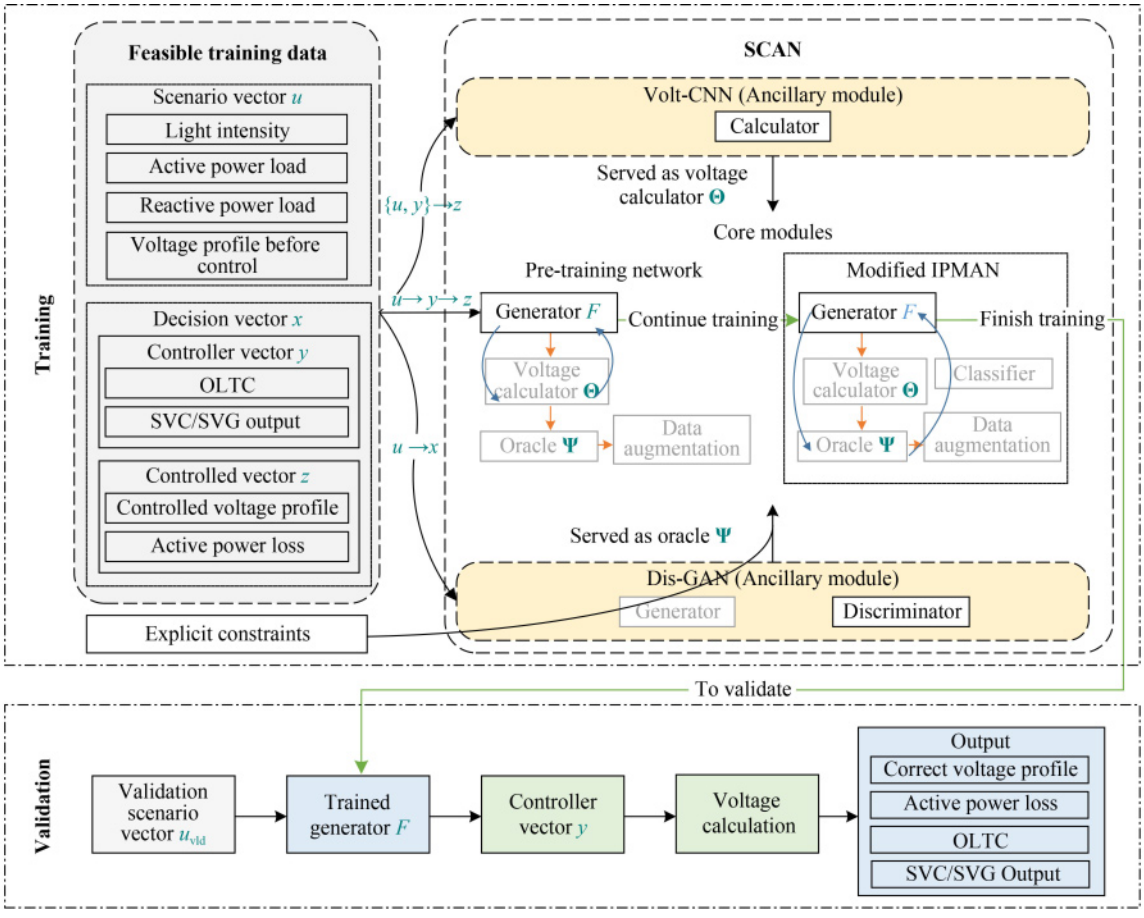

Fig. 5 The structure of the SCAN.

3) The generator F in the Pre-training Network is further trained in Modified IPMAN, where Semi-GAN is used instead of Style-GAN allow for an unlimited number of scenarios. Several loss functions are proposed for the Semi-GAN structure. Additionally, to prevent overfitting, a two-step training strategy is also introduced into Modified IPMAN. After training, the SCAN output is a reliable F.

4) For validation, the decision generator F generates y on the validation scenario vector u_{vld}. Next, $\boldsymbol{\Theta}$ calculates z on u_{vld} and y and outputs the correct voltage profile, active power loss, OLTC, and SVC/SVG output.

4 Novel ancillary modules in SCAN

In this Section, we introduce the two ancillary modules in SCAN in detail. Dis-GAN is a novel GAN module addressed to expand oracle $\boldsymbol{\Psi}$ by manifesting hidden constraints in a discriminator, and Volt-CNN is a novel CNN module serving as the voltage calculator $\boldsymbol{\Theta}$, which is applied to escalate the physical relationship between variables to raise the reliability and credibility of classifier B and the predicted objective value.

4.1 Realizing oracle augmentation via Dis-GAN

As the power factor constraint focuses on the injected power rather than all decision variables, an extra constraint was added to oracle $\boldsymbol{\Psi}$ to improve the capability of classifier B to classify feasible and infeasible data. Considering that the newly added constraint should not change the optimization model established in Section 2, that constraint reflects the hidden constraints. Therefore, Dis-GAN is introduced into SCAN to train a discriminator that can judge whether the decision vector x is feasible for hidden constraints.

Dis-GAN is a typical GAN module, with the same loss function as Eq. (9). A Semi-GAN structure is used for Dis-GAN to avoid the limited scenarios caused by the structure of Style-GAN. Compared with Style-GAN, Semi-GAN works in a relatively traditional way, generating a decision vector from one feature map, instead of the incremental training in Style-GAN (Fig. 6). With the loss function (Eq. (9)) focusing more on the MSE, the scenario and decision vectors have a one-to-one correspondence in the VPI problem, allowing the noise vector to be removed in Semi-GAN.

The resulting trained discriminator can verify whether a decision seems feasible, manifesting the hidden constraints. Together with explicit constraints, it is used as oracle $\boldsymbol{\Psi}$ in core modules.

4.2 Rebuilding physical correlation via Volt-CNN

The decision vector x consists of the outputs of the controllers and controlled objects. We refer to the controller outputs, including OLTC, and SVC/SVG outputs as the controller vector y, while we refer to the controlled objects including voltages and active power loss as controlled vector z. Such decision variables originally share a strong physical correlation; however, in the absence of power flow and constraints of substations with OLTC, from the neural network perspective, variables in x are independent of each other. Despite the MSE loss offering a restraint, some variables in the feature map may still be too large while others are too small. Nevertheless, since the IPMAN classifier just outputs a number, and the veracity of the decision is dependent on whether the number is above 0.5, a clearly infeasible decision may be considered a feasible one. To eschew that problem, we split the issue into two parallel sub-problems by coalescing the knowledge of the power system into SCAN.

For a power distribution network with fixed topology, z is completely dictated by the loads and output of the MGs and controllers, y, and scenario vector u, which share a one-to-one correspondence. Therefore, a module was introduced into SCAN to embody this correspondence, calculating z on u and y as a voltage calculator $\boldsymbol{\Theta}$. Then, the generator F only needs to generate y on u. The significant reduction in the number of generated variables

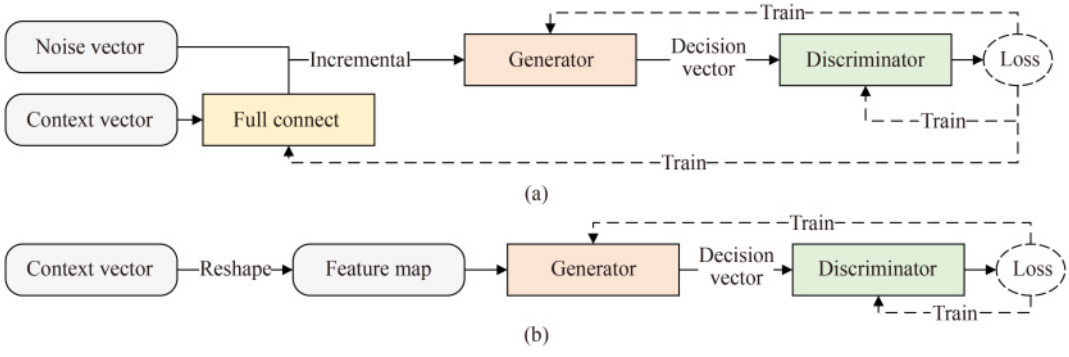

Fig. 6 The structure of (a) Style-GAN and (b) Semi-GAN.

ensures higher reliability. Consequently, a Volt-CNN is imported into SCAN as an ancillary module, and a CNN structure is selected because the buses are susceptible to each other, which meets the CNN flair in handling highly correlated data.

The Volt-CNN is primarily trained on a feasible data set D independently, then it remains untrainable in the Pre-training Network and Modified IPMAN.

5 Enhanced core modules in SCAN

In this Section, we enhanced the core modules in SCAN. By introducing Semi-GAN into SCAN, the number of SCAN scenarios is broadened unlimitedly, and a novel two-step training procedure together with an original loss function $L_{F\text{-noise}}$ is proposed to tackle the issues induced by the introduction of Semi-GAN.

5.1 Generating infeasible data set via Pre-training Network

For a certain scenario vector in a fixed power distribution network, there is one optimal decision vector that shares a one-to-one correspondence; therefore, for the raised VPI problem, a one-shot module with a waterfall training process is sufficient, and it is unnecessary to use the GAN with an alternative training process, which likely increases the computational complexity. Thus, a simplified and enhanced Pre-training Network was proposed to generate the infeasible data set D and individually train the generator F.

The training process of this proposed Pre-training Network is presented in Fig. 7. First, the generator F was built and compiled, and a CNN structure resembling the Volt-CNN was chosen for F in the Pre-training Network. Then, the controller vector y_i was generated according to the scenario vector u_i. Next, the controlled vector z_i was calculated by the voltage calculator $\boldsymbol{\Theta}$ on u_i and y_i. Then, z_i and y_i were combined as the decision vector x_{Pre} and judged by oracle Ψ. If $\Psi(x_{\text{Pre}}, u_i) = 1$, which means x_{Pre} was feasible to that scenario, (x_{Pre}, u_i) was saved for the feasible data set D, otherwise it was saved for the infeasible data set $\underline{D}$. Finally, F is updated based on the MSE loss function, and the process is restarted to generate y_i.

Specifically, the input for F was a three-dimensional figure (Fig. 8), with different data of the same bus set in different layers. Furthermore, light intensity is attached to the end of bus data in each layer. Compared with the traditional one-dimensional vector input, the data placed in different layers preserves the relativity of multi-type data (e.g., active power, reactive power, and voltage profile before control). A square matrix formation is more scrutable to CNN, and well-placed input data eliminate the need for fully connected layers before feeding into the convolutional CNN layer. This accelerates the training and upgrades the performance.

5.2 Broadening the scope of scenarios via modified IPMAN

In modified IPMAN, the Semi-GAN is used instead of Style-GAN; however, the loss function L_F (Eq. (10)) contains MSE, resulting in SCAN being able to only seek optimal decisions from the existing scenario vectors u in the feasible data set D. Consequently, although L_F has a good performance in IPMAN, a new training process and a new loss function are required in the Modified IPMAN inside SCAN.

Since the impracticality comes from the MSE in L_F (Eq. (10)), we can remove it from L_F. We trained F with randomly generated noise u_{noise} instead of the existing scenario vector u to make F able to generate optimal decisions under all scenarios. The loss function is defined as follows:

$$\min_{F\in\mathcal{F}}\left\{L_{F-\text{noise}}=\frac{1}{N_{u,\text{noise}}}\sum_{u_{\text{noise}}\in U_{\text{noise}}}\left(\lambda_j\left[\sum_{m=1}^{n}\beta_m(V_m-1)^2+\alpha P_{\text{loss}}\right]-\sum_{r\in\mathrm{R}}\left[B^{(k)}(F(u_{\text{noise}}),u_{\text{noise}})\right]_r\right)\right\}, \tag{11}$$

where the dual parameter λ_j affects the weight of the objective value in $L_{F\text{-noise}}$, that is, a lower λ_j leads to a more conservative generator, which focuses more on feasibility instead of optimality. The training procedure, denoted as Algorithm 1.

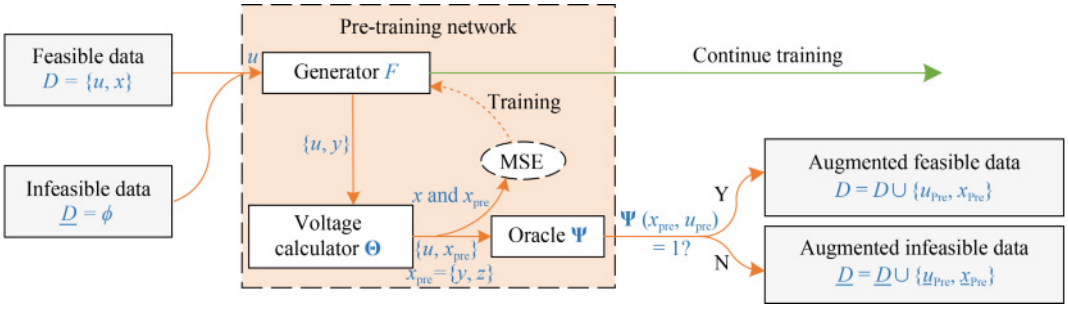

Fig. 7 Training process of pre-training network.

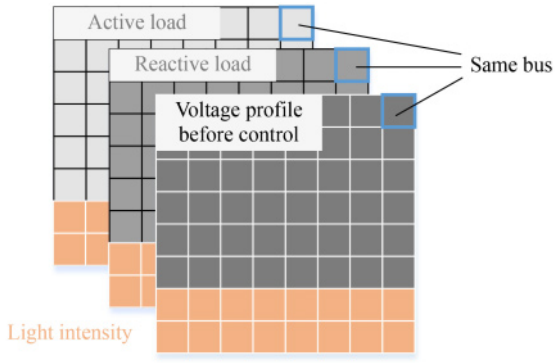

Fig. 8 Layout of training data in F.

Algorithm 1: Modified IPMAN
Data: Generator F, feasible data set D, infeasible data set D, number of outer iterations K, number of middle iterations E_B, E_F
Result: Final generator model F
Train F in Pre-training network;
Initialize Classifier B;
for $k = 1$ **to** K **do**
  Randomly select training data set $D(k)$ and $\underline{D}(k)$ from D and $\underline{D}$;
  for $e = 1$ to E_B do
    Train Classifier B on $D(k)$ and $\underline{D}(k)$;
  end
  for $e = 1$ **to** E_F **do**
    Use randomly generated noise u_{noise} to train Generator F on $L_{F\text{-noise}}$;
    Data augmentation: expand D and $\underline{D}$;
  end
end

To balance optimality and feasibility, the first and second parts of $L_{F\text{-noise}}$ should be consistent within one order of magnitude. The output of B is between 0 and 1. Additionally, considering the decisions are normally feasible, the second part of $L_{F\text{-noise}}$ should be close to 1. Meanwhile, the expected objective function value can be estimated from the training data. The range of proper λ_j is stated as follows:

$$\frac{0.1}{f_{\text{E}}} \leqslant \lambda_j \leqslant \frac{100}{f_{\text{E}}}, \tag{12}$$

where f_{E} stands for the expected objective function value.

Nevertheless, the performance of this training process strongly depends on the voltage calculator $\boldsymbol{\Theta}$ and classifier B. For a small grid with tens of buses, it is relatively simple to get ample pieces of training data covering the entire solution space and giving a high plausibility in the performance of the voltage calculator $\boldsymbol{\Theta}$ and classifier B; however, when it comes to a big grid with hundreds of buses, collecting so much data poses a great challenge. In other conditions, overfitting occurs in modified IPMAN when λ_j is given a large value, weighting the objective value with a gigantic ratio in $L_{F\text{-noise}}$, which leads F to find optimal decisions, and the predicted objective value is far from the true objective value.

Here, another step is added after the first to provide additional guidance for F, which is denoted as Algorithm 2. In this step, F is trained on $(x_i, u_i) \in D$ to curb the overfitting. As each u_i has a corresponding x_i, the MSE can be added back to the loss function, rendering L_F (Eq. (10)) feasible in training. For the raised VPI problem, L_F is written as follows:

$$\min_{F\in\mathcal{F}}\left\{L_F = \frac{1}{N_{\text{u}}}\sum_{u_i\in U}\left(\lambda_j\left[\sum_{m=1}^{n}\beta_m(V_m-1)^2+\alpha P_{\text{loss}}\right]\right.\right.$$
$$\left.\left.+\lambda_{\text{ST}}\left\|F(u_i)-x_i\right\|_1-\sum_{r\in\text{R}}\left[B^{(k)}(F(u_i),u_i)\right]_r\right)\right\}. \tag{13}$$

Algorithm 2: Modified IPMAN with two-step training procedure
Data: Generator F, feasible data set D, infeasible data set $\underline{D}$, number of outer iterations K, number of middle iterations E_B, E_F, number of inner iterations P_{step1}, P_{step2}
Result: Final generator model F
Train F in Pre-training network;
Initialize Classifier B;
for $k = 1$ **to** K **do**
  Randomly select training data set $D(k)$ and $\underline{D}(k)$ from D and $\underline{D}$;
  for $e = 1$ to E_B do
    Train Classifier B on $D(k)$ and $\underline{D}(k)$;
  end
  for $e = 1$ **to** E_F **do**
    for $p = 1$ **to** P_{step1} **do**
      Use randomly generated noise u_{noise} to train Generator F on $L_{F\text{-noise}}$;
    end
    for $p = 1$ to P_{step2} do
      Use $(x_i, u_i) \in D$ to train Generator F on L_F;
    end
    Data augmentation: expand D and $\underline{D}$;
  end
end

Similar to λ_j, the weight of MSE λ_{ST} can be set by the calculation before training. The expected error of each element $e_{\text{estimated}}$ in the decision vector can be estimated as follows:

$$e_{\text{rm}} = \text{inverse}-\text{normalization}\left(\sqrt{\frac{1}{\lambda_{\text{ST}}}}\right). \tag{14}$$

For example, when λ_{ST} was set as 30 and the voltages were normalized on a range from 0.9 to 1.1, $e_{\text{estimated}}$ was approximately 0.037. In practice, the MSE part does not often reach 1, because F is invariably optimizing toward a lower loss function.

When using the two-step procedure, we can make F an aggressive or conservative generator by balancing the

generations of the two steps. For example, we trained F in the first step for four generations and trained it in the second step for one generation, forming two inner iterations. Then, the inner iterations loop in a middle-level iteration. Then carry out the middle-level iteration and the training of B loop in the outer iteration (see Fig. 9) and ensure increasing precision in decision feasibility.

6 Case study

In this Section, we perform case studies on IEEE 33- [30] and 123-bus [31] test systems to demonstrate the effectiveness of the proposed model. These experiments were solved on a personal computer with an Intel Core (i5-11400F, 2.60 GHz) processor and 8 GB of memory. Data generation and result validation are implemented by Matpower 7.1 and Mosek 9.1.9 using MATLAB R2021a. Data processing, model establishment and training are implemented by Tables 3.6.1, numpy 1.18.5, tensorflow 2.7.0 in Python 3.8.

The IEEE 33- and 123-bus system configurations are depicted in Figs. 10 and 11, respectively. The MG locations, SVCs and SVGs are shown in Tables 1 and 2, respectively. Since MGs are not built by DSOs, we randomly chose their locations. Referring to the active load of buses, the PV capacity of each MG is set as 100 kW, except for bus 24 in the IEEE 33-Bus System, whose active load was significantly higher than that of the others. SVCs and SVGs were always set to ensure the local consumption of reactive power; therefore, they were evenly set in the grid and their sizes were standard. Each active and reactive load is timed with an individual factor that randomly fluctuates in the range [0.5, 1.5], while light intensity randomly fluctuates from 0 to 1. The tap settings of OLTC were 0.950, 0.975, 1.000, 1.025, and 1.050, respectively. The nominal voltage of each bus was set as 1. In Eq. (2), the weighting factors α and β_m and the standard voltages V_{m0} were set as 1.

The SCAN input is the power distribution network operating states, containing active and reactive loads of each bus, light intensity, and voltage profile before control. The topology of the power distribution network is assumably inaccurate or missing. The SCAN output is a decision made on power distribution network status, including OLTC and SVC/SVG output.

For the training data set, optimal decisions were generated using Mosek to solve SOCP formed on the

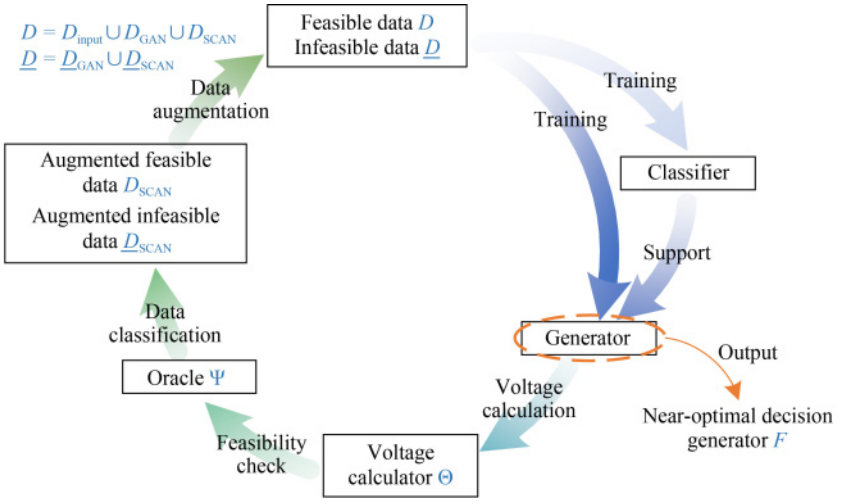

Fig. 9 Outer iteration of Modified IPMAN.

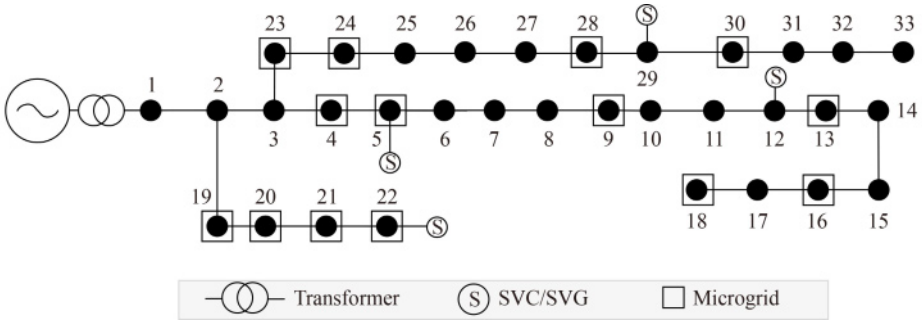

Fig. 10 Topology of IEEE 33-bus system.

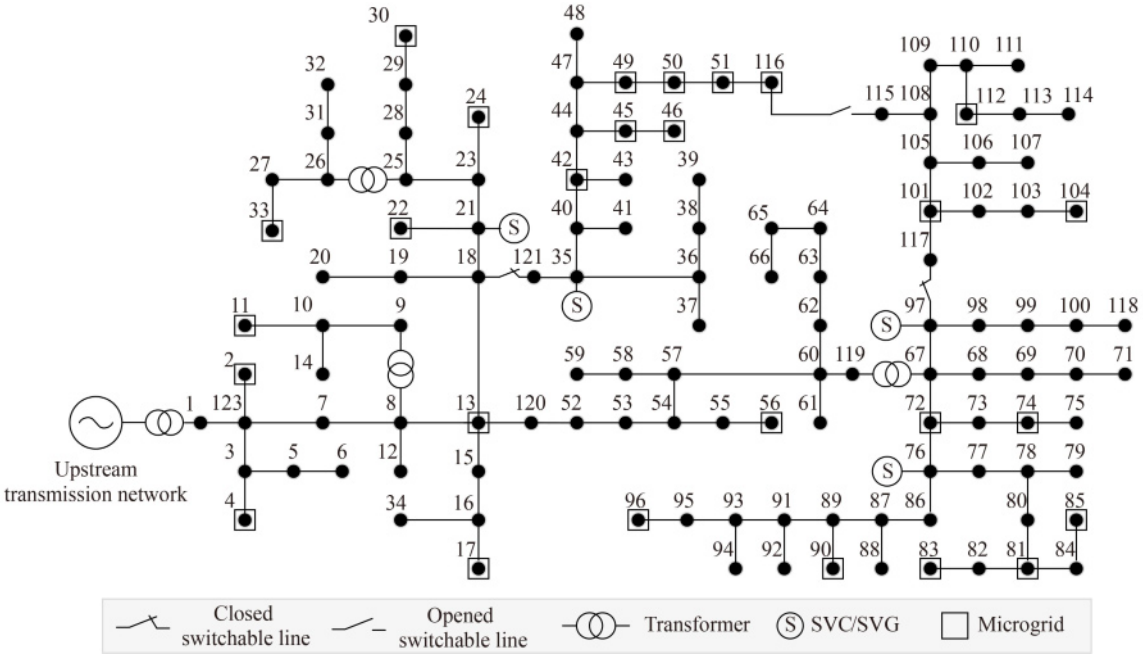

Fig. 11 Topology of IEEE 123-bus system.

Table 1 Buses integrated with MGs

System	Buses integrated with MGs	PV capacity/kW
IEEE 33-bus	4, 5, 9, 12, 13, 16, 19, 21, 22, 23, 28, 30	100
	24	400
IEEE 123-bus	2, 4, 11, 13, 17, 22, 24, 30, 33, 42, 45, 46, 49, 50, 51, 56, 67, 69, 72, 74, 81, 83, 85, 90, 96, 101, 104, 112, 116	100

Table 2 Buses with reactive compensator

System	Reactive compensator type	Buses with compensator	Max output/Mvar	Min output/Mvar
IEEE 33-bus	SVC	5, 29	1	−0.4
	SVG	13, 22	0.5	−0.3
IEEE 123-bus	SVC	21, 76, 97	0.5	−0.3
	SVG	35, 52	0.5	−0.3

dist-flow model. In practice, when the compensator output reached its maximum or minimum value, the operator changed the OLTCs to keep the output away from its ceiling and floor, respectively. To mimic this phenomenon, if there were over two compensators whose outputs reached the maximum or minimum, the OLTCs changed to a lower or higher transformer ratio until the number was lower than two or the OLTCs reaching its floor or ceiling. Finally, as the decisions are made empirically and without topology, the SVC and SVG outputs were added with a number randomly oscillating in the range of [–0.1, +0.1] Mvar. These decisions present the empirical decisions, forming the training data set containing 5000 pieces of feasible data. For the validation data set, the decisions were the worst ones in the SVC and SVG oscillation ranges in empirical decisions, marked as the worst empirical decisions (WEDs). Overall, there were 100 pieces of data in the validation data set.

In the process of testing the methods, decision vectors corresponding to validation data set were generated, and matpower was used to calculate the voltage profile and power loss of the controlled system.

6.1 Performance validation of SCAN

To test the performance of SCAN, we trained the Dis-GAN for 1000 generations, Volt-CNN for 1500 generations, the Pre-training Network for 500 generations. In the Modified IPMAN, the outer iteration was looped for 15 generations, within which classifier B was trained for 50 generations and the middle-level iteration was looped for five generations. For the loss function $L_{F\text{-noise}}$ and L_F, λ_j was set as 100 and λ_{ST} was set

as 30. Since 5000 pieces were sufficient for the 33-bus system, SCAN was trained with Algorithm 1, with only step 1 inside. Accordingly, for the 123-bus system, where the data set was insufficient, it was trained with Algorithm 2, with four generations for each step.

We tested SCAN with the validation data set, and compared it with WED, SOCP, deep neural network (DNN), CNN, and Semi-GAN without Dis-GAN or Volt-CNN (Table 3). All methods were computed in the topology-independent case except for SOCP, which was used to show the true optimal solution.

Juxtaposed with WED, none of the topology-independent methods could guarantee the generated decisions would excel at the empirical decisions, with 10%–20% of the samples being worse than WED. SCAN was slightly better than the other methods from this perspective; however, when it comes to the average and maximum objective value of the 100 pieces of data, a different result emerged. Although those of each method were less than that of WED, SCAN performed far better. The average objective value was 51% less than that of WED in the 33-bus system and 63% in the 123-bus system. For the maximum value, SCAN was 60% less in the 33-bus system and 72% less in the 123-bus system. SCAN showed its advantages in facing various and changing scenarios, validating its ability to make timely decisions. Generally, SCAN performed much better than empirical decisions in both systems.

Compared with SOCP, the mathematical optimization was based on accurate topology in the proposed topology-independent method, SCAN, and was slightly worse in the 33-bus system, that is, 0.019 larger in average objective value and 0.026 larger in maximum objective value. For the 123-bus system, although SCAN improved more from WED in comparison with that in the 33-bus system, there was still a small gap between SCAN and SOCP. That is, SCAN was 0.037 larger than SOCP in average objective value and 0.128 larger in maximum objective value because in the 123-bus system, the number of controllers was significantly larger than that in the 33-bus system and the training data set was worse than that in the 33-bus system.

Focusing on SCAN without Volt-CNN, we found that without Volt-CNN, the results were similar to CNN. Instead of finding a way to minimize the objective function, SCAN without Volt-CNN only imitated the input data set, like other methods. When it comes to SCAN without Dis-GAN, the results were much better than SCAN without Volt-CNN, but still worse than SCAN.

The decisions generated by SCAN could not guarantee that it was better than WED in every scenario. Instead, they kept the objective value below a certain value far less than that of WEDs. In other words, SCAN made decisions that kept the voltage deviation and power loss of the power distribution network at a significantly low level in all test scenarios. Additionally, compared with the incomplete SCAN, we found that both Dis-GAN and Volt-CNN enhance the performance of SCAN while Volt-CNN had a more effective role.

The VPI is listed in Table 4 and shown in Fig. 12, and is similar to that shown in Table 3; however, the maximum objective value of SCAN was larger than that of other AI-based methods because they were calculated

Table 3 The effectiveness of SCAN in overall objective

System	Indicator	WED	SOCP	DNN	CNN	Semi-GAN	SCAN without Dis-GAN	SCAN without Volt-CNN	SCAN
IEEE 33-bus	AOV	0.3687	0.1594	0.3461	0.3273	0.3264	0.2049	0.3354	0.1782
	MOV	0.5420	0.1922	0.4452	0.4042	0.4061	0.2670	0.4073	0.2178
	NSBWED	—	100	67	74	76	88	68	92
IEEE 123-bus	AOV	0.4076	0.1139	0.3826	0.3507	0.3520	0.2370	0.3460	0.1508
	MOV	0.9868	0.1450	0.8824	0.8434	0.8359	0.5109	0.8132	0.2731
	NSBWED	—	100	61	82	81	84	78	86

Notes: AOV–Average objective value; MOV–Maximum objective value; NSBWED–Numbers of samples better than WED.

Table 4 The effectiveness of SCAN in the norm of voltages

System	Indicator	WED	SOCP	DNN	CNN	Semi-GAN	SCAN without Dis-GAN	SCAN without Volt-CNN	SCAN
IEEE 33-bus	AOV	0.1767	0.0098	0.1009	0.0934	0.0934	0.0237	0.1534	0.0115
	MOV	0.2634	0.0231	0.1312	0.1120	0.1177	0.0334	0.2216	0.0223
	NSBWED	–	100	78	80	82	85	76	89
IEEE 123-bus	AOV	0.0845	0.0038	0.0599	0.0554	0.0555	0.0534	0.0792	0.0521
	MOV	0.4822	0.0084	0.1188	0.1049	0.1108	0.1294	0.4356	0.1449
	NSBWED	–	100	38	39	40	48	44	50

Notes: AOV–Average objective value; MOV–Maximum objective value; NSBWED–Numbers of samples better than WED.

on a combined objective function. SCAN had a more balanced focus on the two objectives and achieved a much better result in the overall objective. Additionally, the maximum objective value in the norm of voltages of SCAN was still much smaller than that of WED, at approximately 70.0% smaller. SCAN still showed its ability to keep the voltage norm below a certain value.

As the core modules use Volt-CNN as a voltage calculator, its effectiveness strongly influenced the performance of SCAN and whether DSOs could learn the controlled voltage in advance. Consequently, it was compared with the result calculated by Matpower to find that after training for 1500 generations, the Volt-CNN result (Fig. 13) for each bus deviated at ±0.003 p.u., which proved that Volt-CNN could correctly predict the voltage profile from scenario vector u and controller vector y. However, when comparing the difference within consequences of the two systems, we discovered that the maximum deviation rose from 0.011 to 0.027, illustrating that the correctness of Volt-CNN becomes lower in a bigger system.

6.2 Sensitivity analysis of λ_j

Dual parameter λ_j, which was the weight of objective value in Eqs. (11) and (13), tremendously influenced aggressiveness and conservativeness of SCAN by guiding the training. The effectiveness of various SCANs trained on different λ_j are compared in Table 5. All the SCANs were trained based on the same F generated by the Pre-training Network. We found that SCAN performed best when λ_j was 10 or 100, consistent with the theoretical derivation in Section 5.

When λ_j was too high, the objective value will get a high weight in the loss function, rendering generator F overfit and easier to be trapped in a local optimal solution. Especially, for IEEE 33-bus system, as there

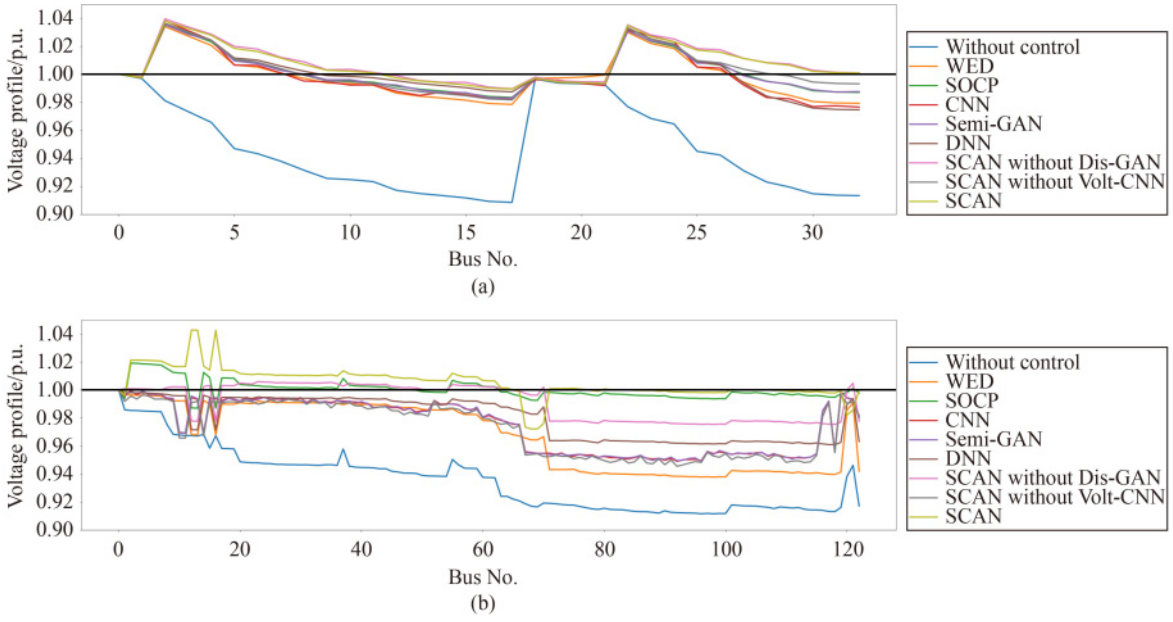

Fig. 12 The effectiveness of SCAN.
(a) IEEE 33-bus system; (b) IEEE 123-bus system.

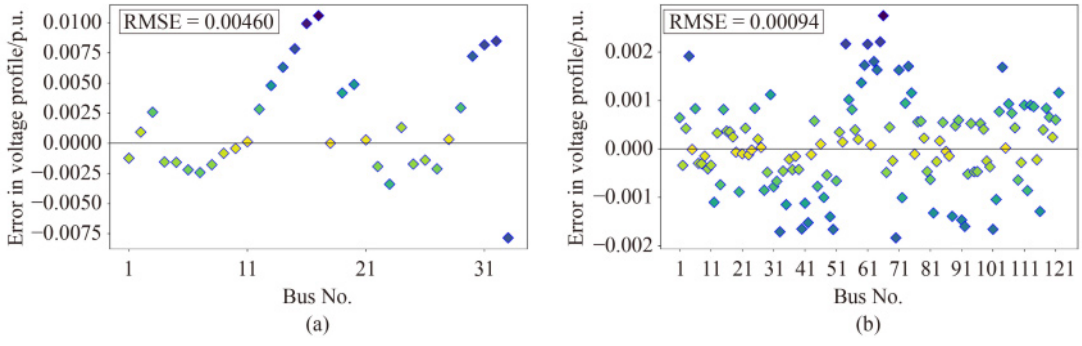

Fig. 13 Prediction error of Volt-CNN.
(a) IEEE 33-bus system; (b) IEEE 123-bus system.

was no second step to provide additional guidance, it came to a detrimental result when λ_j = 1000. When λ_j got lower, the objective value got lower weights in the loss function, rendering SCAN less susceptible to the objective value.

6.3 The role of two-step training

For IEEE 33-bus system, we replaced four generations of step 1 with step 2 in the inner iteration to hold the total training generations fixed. Compare the result with that of eight generations of step 1, illustrated in Table 6. Under most λ_j values, the results trained using this two-step method were worse than those by the one-step method and better than those from WED, proving that additional guidance hindered the way for F to search for optimal results; however, for λ_j = 1000, this two-step method was far better than the one-step method, indicating that the introduction of step 2 can effectively curb over-fitting by offering additional guidance.

For IEEE 123-bus system, we replaced four generations of step 2 with step 1 in the inner iteration and set λ_j to 100 (Table 7). When the one-step training procedure was used, both the average and maximum objective values were worse than those from WED. This was caused by the insufficiency of the training data. For IEEE 33-bus system, there were 65 parameters fluctuating and 5000 pieces of data covered the whole area; however, when it comes to the IEEE 123-bus system, there were 171 parameters fluctuating, rendering 5000 pieces of data insufficient for SCAN to learn the decisions on its own. The different results generated by the one- and two-step training methods indicate that the introduction of step 2 offered additional guidance and mitigated the adverse effect originating from the insufficiency of training data.

To summarize, this step 2 was the insurance for SCAN, that is, if each parameter was set soundly and training data were adequate, step 2 thwarted SCAN from getting the optimal decision. However, in other conditions, step 2

Table 5 Influence of λ_j on SCAN

System	Indicator	WED	λ_j				
			1000	100	10	1	0.1
IEEE 33-bus	AOV	0.3687	0.5941	0.1782	0.1897	0.1967	0.2383
	MOV	0.5420	0.7136	0.2178	0.2406	0.2498	0.2990
	NSBWED	–	0	92	89	89	77
IEEE 123-bus	AOV	0.4076	0.1651	0.1508	0.1357	0.1860	0.2654
	MOV	0.9868	0.3873	0.2731	0.1812	0.5285	0.6822
	NSBWED	–	79	86	87	74	58

Notes: AOV–Average objective value; MOV–Maximum objective value; NSBWED–Numbers of samples better than WED.

Table 6 Comparison between different training procedures for IEEE 33-bus system

Training step	Indicator	WED	λ_j				
			1000	100	10	1	0.1
Step 1 : Step 2 = 8 : 0	AOV	0.3687	0.5941	0.1782	0.1897	0.1967	0.2383
	MOV	0.5420	0.7136	0.2178	0.2406	0.2498	0.2990
	NSBWED	—	0	92	89	89	77
Step 1 : Step 2 = 4 : 4	AOV	0.3687	0.3230	0.3222	0.3256	0.3241	0.3295
	MOV	0.5420	0.4076	0.4071	0.4034	0.4078	0.4092
	NSBWED	—	75	75	73	72	70

Notes: AOV–Average objective value; MOV–Maximum objective value; NSBWED–Numbers of samples better than WED.

Table 7 Comparison between different training procedures for IEEE 123-bus system (λ_j = 100)

Indicator	WED	Step 1 : Step 2 = 8 : 0	Step 1 : Step 2 = 4 : 4
AOV	0.4076	0.5636	0.1508
MOV	0.9868	1.5998	0.2731
NSBWED	–	58	86

Notes: AOV–Average objective value; MOV–Maximum objective value; NSBWED–Numbers of samples better than WED.

Table 8 Test results considering topology changing

Indicator	18–121 and 115–116		97–117 and 115–116		18–121 and 97–117	
	WED	SCAN	WED	SCAN	WED	SCAN
AOV	0.1305	0.152	0.1746	0.1800	0.1486	0.1578
MOV	0.2282	0.2473	0.4032	0.2550	0.2792	0.2390
NSBWED	–	40	–	34	–	47

Notes: AOV–Average objective value; MOV–Maximum objective value; NSBWED–Numbers of samples better than WED.

offered additional guidance by the MSE part in L_F, ensuring that SCAN found a better decision instead of the optimal decision.

6.4 Adaptability to topology changing

Although the topology may not change frequently when the DSO cannot get an accurate one, we further tested the adaptability of SCAN on these extended scenarios. A training data set of the IEEE-123 bus system considering topology variations was generated. The switchable lines were randomly open or closed while keeping the topology radiality of the system. For each combination of switch status, we generated a test data set containing 100 pieces of data. SCAN was trained as described in Section 6.1 (Table 8). When the topology changing is taken into consideration, SCAN shows slightly worse results in both average objective value and numbers of samples better than WED; however, in the maximum objective value among the 100 test samples, SCAN shows its ability to improve it. When the closed switchable lines are 97–117 and 115–116, SCAN reduces the maximum from 0.4032 to 0.2550, meanwhile, for 18–121 and 97–117, the performance is from 0.2792 to 0.2390.

Although currently SCAN cannot clearly recognize the topology changing, it can still keep the objective value consistently below a certain value.

7 Conclusions

This paper proposes a novel end-to-end model called SCAN to solve the VPI problem from a topology-independent view. SCAN aimed to solve the VPI problem in power distribution networks integrated with MGs, with an unlimited number of scenarios. Several novel loss functions were proposed to serve SCAN. To overcome the inadequacy of explicit constraints, Dis-GAN was introduced to SCAN, forming an explicit constraint reflecting the hidden constraints. Considering the strong physical correlation between the variables, the Volt-CNN was interposed to the SCAN as a voltage calculator to improve the performance. Several case studies were applied to the IEEE 33- and 123-bus systems, testing SCAN on 100 randomly generated samples. SCAN is over 50% less than WED in both maximum and average objective value among those samples, and less than other methods, showing the ability of SCAN to keep the objective values steadily at a significantly lower level under various scenarios. SCAN can also be applied when the topology is changing and can always provide a solution that significantly improves the voltage profile in the power distribution network. Volt-CNN shows a high precision, with a deviation remaining in ±0.003 p.u., which enables DSOs to know the controlled voltage profile in advance. Additionally, Volt-CNN brings SCAN a brilliant performance, resulting in objective indicators over 40% less than those of SCAN without Volt-CNN. The mechanism of the two-step training procedure is clarified by the comparison of results generated by different training procedures.

As an emerging field of research, the end-to-end deep learning method shows its broad applicability and excellent performance in power engineering. For further research, more application scenarios in the context of power distribution networks will be explored to realize the one-shot direct control from data to decisions.

Acknowledgment This work was funded by the National Natural Science Foundation of China (Grant Nos. 52007164, U2066601).

References

1. Mahdavi S, Panamtash H, Dimitrovski A, et al. Predictive coordinated and cooperative voltage control for systems with high penetration of PV. IEEE Transactions on Industry Applications, 2021, 57(3): 2212–2222
2. Ajoulabadi A, Ravadanegh S N, Mohammadi-Ivatloo B. Flexible scheduling of reconfigurable microgrid-based distribution networks considering demand response program. Energy, 2020, 196: 117024
3. Wang Y, Huang Z, Shahidehpour M, et al. Reconfigurable distribution network for managing transactive energy in a multi-microgrid system. IEEE Transactions on Smart Grid, 2020, 11(2): 1286–1295
4. Liu J H, Cheng J S. Online voltage security enhancement using voltage sensitivity-based coherent reactive power control in multi-area wind power generation systems. IEEE Transactions on Power Systems, 2021, 36(3): 2729–2732
5. Liu J, Xu Y, Dong Z Y, et al. Retirement-driven dynamic VAR planning for voltage stability enhancement of power systems with high-level wind power. IEEE Transactions on Power Systems,

2018, 33(2): 2282–2291
6. Ardakanian O, Wong V W, Dobbe R, et al. On identification of distribution grids. IEEE Transactions on Control of Network Systems, 2019, 6(3): 950–960
7. Zhang H, Zhao J, Wang X, et al. Low-voltage distribution grid topology identification with latent tree model. IEEE Transactions on Smart Grid, 2022, 13(3): 2158–2169
8. Su C T, Lin C T. Fuzzy-based voltage/reactive power scheduling for voltage security improvement and loss reduction. IEEE Transactions on Power Delivery, 2001, 16(2): 319–323
9. Nguyen T T, Truong A V. Distribution network reconfiguration for power loss minimization and voltage profile improvement using Cuckoo search algorithm. International Journal of Electrical Power & Energy Systems, 2015, 68: 233–242
10. Wang C, Liu Y, Zhao Y, et al. A hybrid topology scale-free Gaussian-dynamic particle swarm optimization algorithm applied to real power loss minimization. Engineering Applications of Artificial Intelligence, 2014, 32: 63–75
11. Elmachtoub A N, Grigas P. Smart "predict, then optimize". Management Science, 2022, 68(1): 9–26
12. Mandi J, Demirović E, Stuckey P J, et al. Smart predict-and-optimize for hard combinatorial optimization problems. Proceedings of the AAAI Conference on Artificial Intelligence, 2020, 34(02): 1603–1610
13. Babier A, Chan T C, Diamant A, et al. Learning to optimize with hidden constraints. arXiv preprint, arXiv:1805.09293, 2018
14. Han J, Yan L, Li Z. A task-based day-ahead load forecasting model for stochastic economic dispatch. IEEE Transactions on Power Systems, 2021, 36(6): 5294–5304
15. Lu C, Jiang W, Wu C. Effective end-to-end learning framework for economic dispatch. IEEE Transactions on Network Science and Engineering, 2022, 9(4): 2673–2683
16. Zhang J, Wang Y, Hug G. Cost-oriented load forecasting. Electric Power Systems Research, 2022, 205: 107723
17. Olivares D E, Mehrizi-Sani A, Etemadi A H, et al. Trends in microgrid control. IEEE Transactions on Smart Grid, 2014, 5(4): 1905–1919
18. Zuo Y, Yuan Z, Sossan F, et al. Performance assessment of grid-forming and grid-following converter-interfaced battery energy storage systems on frequency regulation in low-inertia power grids. Sustainable Energy, Grids and Networks, 2021, 27: 100496
19. Pattabiraman D, Lasseter R, Jahns T. Comparison of grid following and grid forming control for a high inverter penetration power system. In: 2018 IEEE Power & Energy Society General Meeting (PESGM), Portland, USA, 2018
20. Poolla B K, Gros D, Dorfler F. Placement and implementation of grid-forming and grid-following virtual inertia and fast frequency response. IEEE Transactions on Power Systems, 2019, 34(4): 3035–3046
21. Yuan H, Xin H, Wu D, et al. Assessing maximal capacity of grid-following converters with grid strength constraints. IEEE Transactions on Sustainable Energy, 2022, 13(4): 2119–2132
22. Denis G, Prevost T, Debry M S, et al. The Migrate project: the challenges of operating a transmission grid with only inverter-based generation. A grid-forming control improvement with transient current-limiting control. IET Renewable Power Generation, 2018, 12(5): 523–529
23. Abujubbeh M, Fahrioglu M, Al-Turjman F. Power loss reduction and voltage enhancement via distributed photovoltaic generation: case study in North Cyprus. Computers & Electrical Engineering, 2021, 95: 107432
24. Abdel-Mawgoud H, Kamel S, Tostado M, et al. Optimal installation of multiple DG using chaotic moth-flame algorithm and real power loss sensitivity factor in distribution system. In: 2018 International Conference on Smart Energy Systems and Technologies (SEST), Seville, Spain, 2018
25. Ruan H, Gao H, Liu Y, et al. Distributed voltage control in active distribution network considering renewable energy: a novel network partitioning method. IEEE Transactions on Power Systems, 2020, 35(6): 4220–4231
26. Wu W, Tian Z, Zhang B. An exact linearization method for OLTC of transformer in branch flow model. IEEE Transactions on Power Systems, 2017, 32(3): 2475–2476
27. Gan L, Low S H. Optimal power flow in direct current networks. IEEE Transactions on Power Systems, 2014, 29(6): 2892–2904
28. Chai Y, Guo L, Wang C, et al. Hierarchical distributed voltage optimization method for HV and MV distribution networks. IEEE Transactions on Smart Grid, 2020, 11(2): 968–980
29. Karras T, Laine S, Aila T. A style-based generator architecture for generative adversarial networks. In: Proceedings of the IEEE/CVF Conference on Computer Vision and Pattern Recognition, 2019, 4401–4410
30. Baran M E, Wu F F. Network reconfiguration in distribution systems for loss reduction and load balancing. IEEE Power Engineering Review, 1989, 9(4): 101–102
31. Schneider K P, Mather B, Pal B, et al. Analytic considerations and design basis for the IEEE distribution test feeders. IEEE Transactions on Power Systems, 2018, 33(3): 3181–3188